THE JOURNAL OF PHYSICAL CHEMISTRY A

pubs.acs.org/JPCA Article

Computational Study Investigating the Atmospheric Oxidation Mechanism and Kinetics of Dipropyl Thiosulfinate Initiated by OH Radicals and the Fate of Propanethiyl Radical

Parandaman Arathala and Rabi A. Musah*

Cite This: *J. Phys. Chem. A* 2020, 124, 8292−8304 Read Online

ACCESS | Metrics & More | Article Recommendations | Supporting Information

ABSTRACT: The OH radical-initiated atmospheric oxidation mechanism of dipropyl thiosulfinate ($CH_3CH_2CH_2-S(O)S-CH_2CH_2CH_3$, DPTS), a volatile released by *Allium* genus plants, has been investigated using *ab initio*/DFT electronic structure calculations. The DPTS + $^{\bullet}$OH reaction can proceed through (1) abstraction and (2) substitution pathways. The present calculations show that addition of $^{\bullet}$OH to the sulfur atom of the sulfinyl (−S(=O)) group, followed by simultaneous cleavage of the S−S single bond, leading to the formation of propanethiyl radical (PTR) and propanesulfinic acid, is the major pathway when compared to the other possible abstraction and substitution reactions. The barrier height for this reaction was computed to be −5.4 kcal mol^{-1} relative to that of the separated DPTS + $^{\bullet}$OH reactants. The rate coefficients for all the possible pathways for DPTS + $^{\bullet}$OH were explored by RRKM-ME calculations using the MESMER kinetic code in the atmospherically relevant temperatures T = 200−300 K and the pressure range of 0.1−10 atm. The calculated total rate coefficient for the DPTS + $^{\bullet}$OH reaction was found to be 1.7×10^{-10} cm^3 molecule^{-1} s^{-1} at T = 300 K and P = 1 atm. The branching ratios and atmospheric lifetime of DPTS + $^{\bullet}$OH were also determined in the studied temperature range. In addition, electronic structure calculations on the multichannel reactions of PTR with atmospheric oxygen ($^3O_2$) were investigated using the same level of theory. The calculations showed that unimolecular elimination of hydroperoxyl radical (HO_2) from the RO_2 adduct through formation of propanethial is a major reaction under atmospherically relevant conditions. The overall results suggest that the atmospheric removal of DPTS is mainly due to reactions with $^{\bullet}$OH and $^3O_2$, resulting in formation of propanesulfinic acid, propanethial, HO_2, and sulfur dioxide (SO_2) as the major products. The atmospheric lifetime of DPTS was estimated to be less than 2 h in the studied temperature range. Estimations of the global warming potential of DPTS and the products of its reaction with $^{\bullet}$OH reveal that while the contribution made by DPTS to global warming is negligible, the various products formed as a consequence of its interaction with OH radical may make substantial contributions to global warming, acid rain, and formation of secondary organic aerosols.

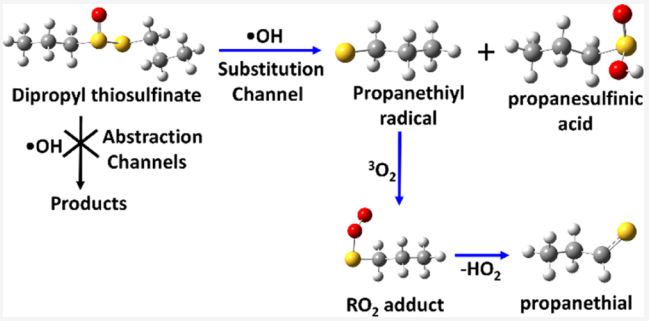

1. INTRODUCTION

Volatile organosulfur compounds (VOSCs) have been the focus of significant attention in recent years because of their contribution to the atmospheric sulfur budget. These compounds play an important role in atmospheric and combustion chemistry, mainly in the formation of aerosols, and elimination of sulfur compounds from crude oil or coal.[1,2] They are also known to participate in global warming, acid precipitation, and cloud formation.[3] The contribution to the atmospheric sulfur burden from natural sources, such as volcanoes, plant and animal decay, marine algae, inland bodies of water, soil, bacteria, and so on, is estimated to be 0.47−2.2 Tmol S year^{-1}.[3,4] Various models have been made to develop a global sulfur cycle, but all of them underestimate the significant amounts of biogenic sulfur needed to balance the global sulfur cycle.[5] Over the last three decades, our knowledge of biogenic sulfur emissions from the sea has improved significantly.[3,6] We now have a reasonably clear picture of the amounts of sulfur emitted from the oceans and their atmospheric fate. In contrast, information regarding terrestrial biogenic sulfur emission sources seems to represent the largest uncertainty in the global sulfur budget. Specifically, VOSCs released from living vascular plants and their removal from the atmosphere are not well understood. This uncertainty is mainly due to the diversity of sulfur compounds emitted, which include hydrogen sulfide (H_2S), sulfur dioxide (SO_2), carbonyl sulfide (COS), carbon disulfide (CS_2), methanethiol (CH_3SH), dimethyl

Received: June 8, 2020
Revised: August 11, 2020
Published: August 29, 2020

https://dx.doi.org/10.1021/acs.jpca.0c05200
J. Phys. Chem. A 2020, 124, 8292−8304

sulfide (DMS), dimethyl sulfoxide (DMSO), and dimethyl sulfone ($DMSO_2$).[6]

DMS and H_2S have been proposed to be the two primary sulfur species emitted by plants.[7−9] However, various thiosulfinates and other sulfur compounds were detected in the atmosphere of a beech forest with *Allium ursinum* as the ground cover.[10] The concentrations ranged from 0.3 to 7.8 ppm, with an average level of 2.9 ppb. The highest mean emission rate of 62 μg S m^{-2} h^{-1} was reported for organic sulfur species emitted from a terrestrial plant.[10] These high concentration levels of VOSCs released from various sources into the troposphere are expected to be removed via photolysis and reactions with atmospheric oxidants such as $^{\bullet}OH$, $^{\bullet}Cl$, NO_x, and ozone (O_3).

Several studies have reported that thiosulfinates such as dimethyl thiosulfinate ($CH_3-S(O)S-CH_3$, DMTS), dipropyl thiosulfinate ($CH_3CH_2CH_2-S(O)S-CH_2CH_2CH_3$, DPTS), propyl methyl thiosulfinate, diphenyl thiosulfinate, and diallyl thiosulfinate are emitted from various *Allium* genus cash crops such as garlic and onions that occupy large acreage on farmlands.[11,12] This raises the question of whether the farming of these crops and their emission of organosulfur compounds into the atmosphere results in organosulfur "hotspots" that may contribute to global warming. Recently, our group has investigated the atmospheric fate of DMTS with $^{\bullet}OH/^{\bullet}Cl$ radicals using high-level electronic structure calculations.[13] The atmospheric oxidation of DMTS that occurs through its interaction with $^{\bullet}OH$ can in principle proceed via abstraction and/or substitution pathways. Because the asymmetry of the molecule makes its two methyl groups different, there are two possible $^{\bullet}OH$-initiated hydrogen abstraction pathways described by eqs 1 and 2.

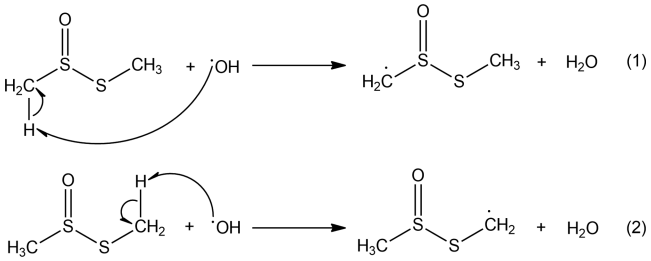

The possible substitution reactions of DMTS + $^{\bullet}OH$ include $^{\bullet}OH$ attack on the S-atom sulfinyl group ($-S(=O)$), followed by $S(=O)-S$ or $C-S(=O)$ single bond fission (eqs 3 and 4) and $^{\bullet}OH$ attack either above or below the plane of the S-atom, followed by $S(=O)-S$ single bond cleavage as described by eq 5.

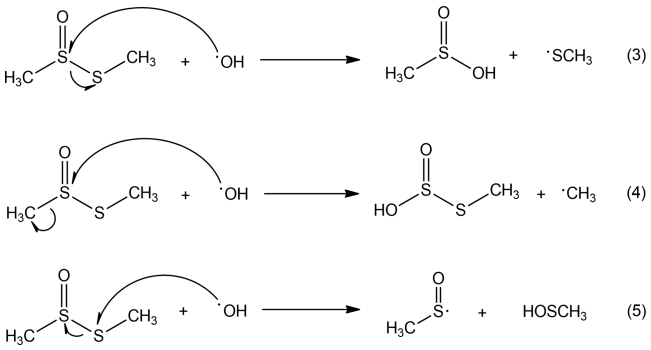

The results from the DMTS + $^{\bullet}OH$ study suggested that $^{\bullet}OH$ addition to the sulfur atom of the sulfinyl group ($-S(=O)$) of DMTS, followed by $S-S(=O)$ single bond fission to form methanesulfinic acid and the methanethiyl radical (i.e. eq 3) is the most favorable of the five available reaction paths. The total rate coefficient for the DMTS + $^{\bullet}OH$ reaction at 300 K was reported to be $k = 1.4 \times 10^{-11}$ cm^3 $molecule^{-1}$ s^{-1}.[13]

The emission of DPTS, a structural analogue of DMTS, from terrestrial plants has led to increased interest in determining the reaction mechanisms and kinetics of its degradation in the atmosphere. The main focus of the present work was the question of how the atmospheric fate of DPTS is impacted by interaction with OH radicals. This compound, which is also called as *S*-propyl-1-propanethiosulfinate, is commonly observed in onion (*Allium cepa*), shallot (*Allium fistulosum*), and several other *Allium* genus plants.[12] On release into the troposphere, it is anticipated that it would undergo reactions with $^{\bullet}OH$.[14−16] In principle, the atmospheric oxidation of DPTS in the presence of $^{\bullet}OH$ could proceed via the two main reaction paths that were available to DMTS, namely, (1) abstraction and (2) substitution. The possible abstraction and substitution pathways of DPTS + $^{\bullet}OH$ are given below in eqs 6−14. Eqs 6−11 show the abstraction of a

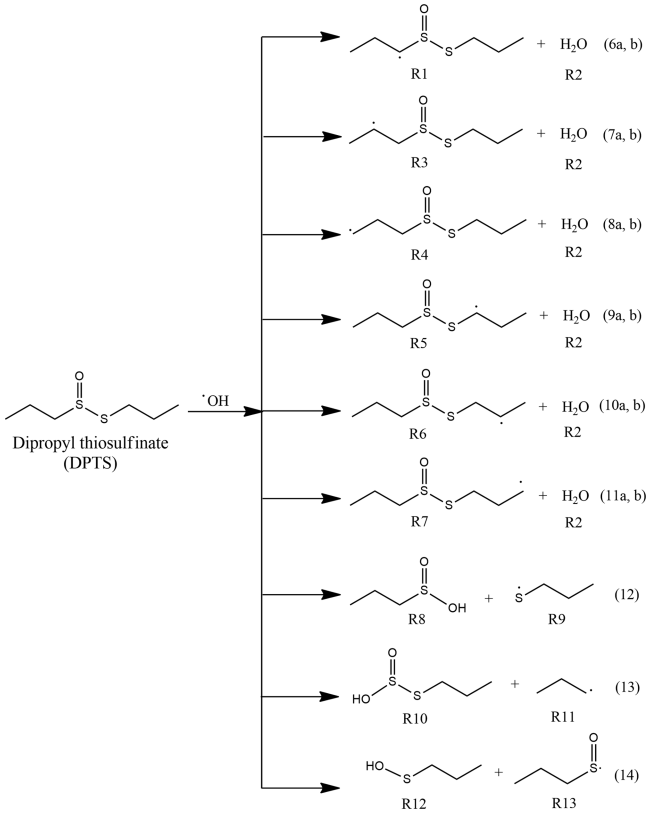

hydrogen atom from $-CH_2$ and $-CH_3$ moieties by $^{\bullet}OH$ at various sites within DPTS. The remaining reactions 12−14 represent the substitution pathways that can proceed by: (1) addition of $^{\bullet}OH$ to the sulfur atom of the sulfinyl ($-S(=O)$) group, followed by simultaneous cleavage of either the $S(=O)-S$ or $C-S(=O)$ single bonds (eqs 12 and 13, respectively); or (2) addition of $^{\bullet}OH$ above or below the plane of the S-atom, followed by simultaneous cleavage of the $S(=O)-S$ single bond (eq 14), forming the corresponding products.

https://dx.doi.org/10.1021/acs.jpca.0c05200
J. Phys. Chem. A 2020, 124, 8292−8304

To date, there are no reports in the literature investigating the atmospheric oxidation mechanism, energetics, and kinetics of DPTS initiated by OH radical. Therefore, we investigated this reaction using electronic structure calculations in conjunction with the MESMER kinetic code.[17] The rate coefficients were calculated over the 200−300 K temperature range and a 0.1−10 atm pressure range. Using the present theoretical results, the oxidation of DPTS and its atmospheric implications are discussed.

2. COMPUTATIONAL METHODS

The electronic structure calculations of the atmospheric oxidation of DPTS with •OH were performed using the Gaussian 16 suite quantum chemistry program.[18] The geometry optimization and frequency calculations of all the minima on the potential energy surfaces (PESs) were computed using the M06-2X density functional method in combination with the 6-311++G(3df,3pd) basis set. Various studies have indicated that this functional can be used for calculation of thermodynamic properties, barrier heights, and noncovalent interactions.[19−21] The M06-2X method is a hybrid meta density functional with a high percentage of HF exchange. This broadly applicable functional can be used for calculating the thermochemical, barrier height, and noncovalent interactions[22] with average mean absolute errors of ∼1.3, 1.2, and 0.5 kcal mol^{-1}, respectively. The large 6-311++G(3df,3pd) Pople type basis set was selected based on its excellent performance in estimating accurate binding energies of complexes when it is used in combination with the M06-2X functional.[13,20] The transition states (TSs) and all other local minima are identified based on the number of imaginary frequencies. All the local minima have only real frequencies, and TSs have a single imaginary vibrational frequency that corresponds to the expected motion along the reaction coordinate. Intrinsic reaction coordinate (IRC) calculations[23,24] were performed at the same level of theory to confirm the obtained TSs connected with their corresponding prereactive and postreactive complexes, respectively. Single-point energy calculations were performed at the coupled-cluster singles and doubles, augmented by a perturbative treatment of triple excitation (CCSD(T)) level, in conjunction with a cc-pVTZ basis set on the M06-2X optimized geometries.[25] The calculated total electronic energies (E_{total}) and zero-point energy (ZPE)-corrected electronic energies [E_{total}(ZPE)] for all the minima obtained at the M06-2X and CCSD(T) levels are given in Table S1. The relative energies, geometries, imaginary frequencies of various TSs, vibrational frequencies, and rotational constants are provided in Tables S2−S6. The spin contamination for all the stationary points present in the DPTS + •OH reaction system was monitored. The anticipated values of the total spin $\langle S^2 \rangle$ were estimated to be between 0.75 and 0.77, which is within a 3% range of the expected value of 0.75. Severe spin contamination could possibly lead to a poorer estimation of the barrier height.[26,27] However, the spin contamination in the present work is found to be negligible.

3. RESULTS AND DISCUSSION

We first investigated the possible conformers of DPTS to determine the most stable geometry in the atmosphere. The structure of DPTS shown in Figure 1 indicates five conformational degrees of freedom, a consequence of the internal rotation about the S2−C3, C3−C6, S2−S23, S23−C13, and C13−C16 single bonds. The potential energy scan calculations were performed using these five dihedral angles at the M06-2X/6-31+G(d,p) level of theory. These computations revealed a total of 67 possible conformers. The obtained conformer geometries were further optimized and characterized with frequency calculations at the M06-2X/6-311++G(3df,3pd) level. Based on the energies of each conformer, the most stable conformer of DPTS was found to be that shown in Figure 1. The high stability of this structure compared to other conformations is mostly due to the additional weak intramolecular hydrogen bonding interactions that exist between the atoms O1···H7 and O1···H14, with their corresponding bond lengths of ∼2.71 and ∼2.75 Å, respectively. This is illustrated by the dotted lines shown in Figure 1. We investigated the reaction mechanism of DPTS + •OH using this conformer.

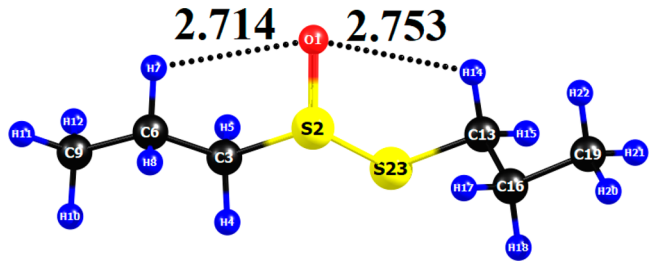

Figure 1. Optimized stable conformer of DPTS calculated at the M06-2X/6-311++G(3df,3pd) level of theory.

3.1. Stationary Points on the PES and Barrier Heights.

We chose to use density functional theory (M06-2X) for geometry optimization and frequency calculations for all the stationary points involved in the DPTS + •OH reaction pathways. This was done because of the excellent performance, computational cost, and high-accuracy results.[13,28,29] Using the M06-2X density functional, the first step was to determine the best estimates of the barrier heights. For this reason, we carried out single-point calculations at the CCSD(T)/cc-pVTZ level on the M06-2X/6-311++G(3df,3pd) optimized geometries.[25]

As discussed in the introduction, the mechanism of DPTS + •OH can proceed via two different classes of reactions, namely, hydrogen abstraction and substitution pathways. The abstraction pathways involve a total of fourteen hydrogen atoms located on the two propyl ($CH_3-CH_2-CH_2-$) moieties attached to the sulfinyl ($-S(=O)$) and $-S-$ atoms, respectively, which should in principle provide 14 different TSs. The M06-2X energy calculations found only 12 different TSs. This is mainly because of the two $-CH_3$ groups of the propyl moieties. While there are a total of six hydrogen atoms involved, each $-CH_3$ has two H atoms that are equivalent and one that is different. This results in a total of four TSs from the two methyl groups, which were labeled as TS5, TS6, TS11, and TS12. In addition, the four $-CH_2$ groups within the propyl moieties involve eight hydrogen atoms. None of them are equivalent, suggesting eight different TSs. They were designated as TS1, TS2, TS3, TS4, TS7, TS8, TS9, and TS10. In total, this yields 12 possible distinct hydrogen abstraction TSs with the hydrogen's involved illustrated below.

In the case of the substitution pathways, •OH addition can occur either above or below the plane of the −S− atom of DPTS via TSs labeled TS13 and TS14, to form propanesulfenic acid ($CH_3-CH_2-CH_2-S-OH$) and the propylsul-

https://dx.doi.org/10.1021/acs.jpca.0c05200
J. Phys. Chem. A 2020, 124, 8292−8304

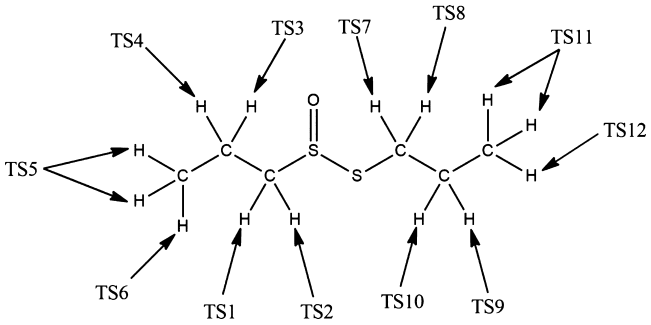

finyl radical ($CH_3-CH_2-CH_2-S^{\bullet}(=O)$) as products. The other two possible substitution channels include addition of $^{\bullet}OH$ to the sulfinyl ($-S(=O)$) moiety, followed by simultaneous bond cleavage on either side of the $-S(=O)$ group, resulting in the formation of: (1) the propanethiyl ($CH_3-CH_2-CH_2-S^{\bullet}$) or (2) the propyl ($CH_3-CH_2-CH_2^{\bullet}$) radical. Their associated TSs are denoted by TS15 and TS16, respectively. Therefore, a total of four substitution TSs are possible for the DPTS + $^{\bullet}OH$ reaction system.

The PESs for the hydrogen abstraction and substitution channels of the DPTS + $^{\bullet}OH$ reaction obtained at the CCSD(T)/cc-pVTZ//M06-2X/6-311++G(3df,3pd) level are shown in Figures 2–4. The optimized geometries of the

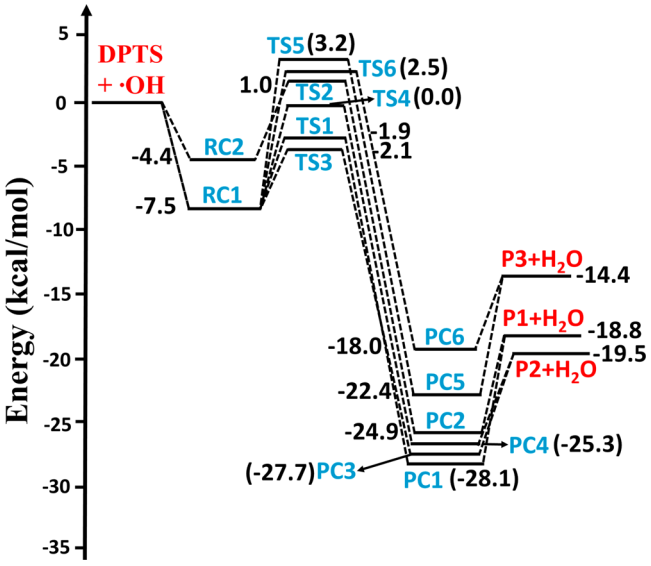

Figure 2. PES diagram for the hydrogen abstraction by •OH from the $CH_3-CH_2-CH_2-S(=O)$ moiety of DPTS. The energies of the stationary points were obtained at the CCSD(T)/cc-pVTZ//M06-2X/6-311++G(3df,3pd) level of theory. The symbols RC*n* (*n* = 1, 2) refer to prereactive complexes; TS*n* (*n* = 1–6) refers to TSs, and PC*n* (*n* = 1–6) refers to postreactive complexes.

reactants, TSs, RCs, and PCs involved in the DPTS + $^{\bullet}OH$ reaction system obtained at the M06-2X/6-311++G(3df,3pd) level are shown in Figure 5 and Figure S1 of the Supporting Information. From Figures 2–4, it is apparent that the abstraction and substitution pathways initially proceed via formation of a stable prereactive complex by association of the two reactants DPTS and $^{\bullet}OH$. This then advances via a finite barrier through a TS to ultimately form a postreactive complex and the bimolecular products. Figure 2 shows the PESs associated with the various $^{\bullet}OH$-mediated hydrogen abstraction channels from the propyl ($CH_3-CH_2-CH_2-$) group

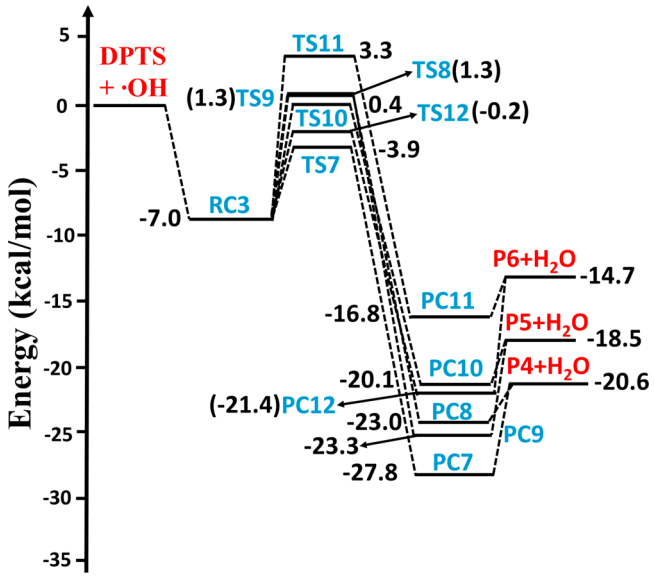

Figure 3. PES diagram for the hydrogen abstraction by $^{\bullet}OH$ from the $CH_3-CH_2-CH_2-S$ moiety of DPTS. The energies of the stationary points were obtained at the CCSD(T)/cc-pVTZ//M06-2X/6-311++G(3df,3pd) level of theory. The symbol RC3 refers to the prereactive complex; TS*n* (*n* = 7–12) refers to TSs, and PC*n* (*n* = 7–12) refers to postreactive complexes.

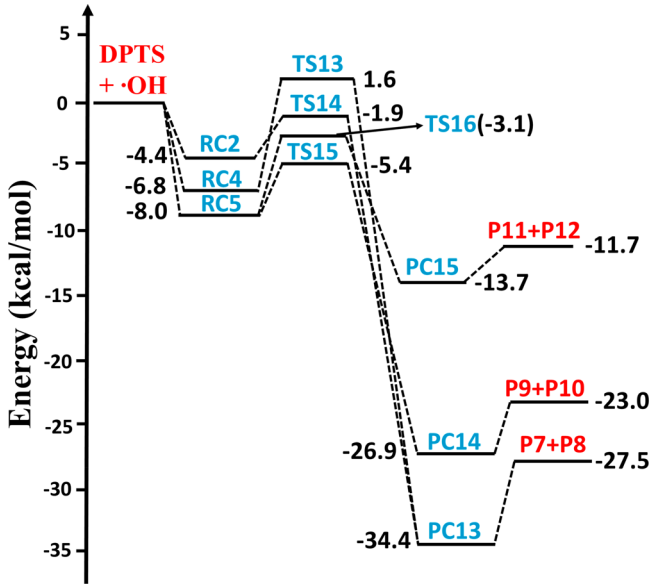

Figure 4. PES diagram for the various $^{\bullet}OH$ substitution channels involved in the DPTS + $^{\bullet}OH$ reaction, leading to the formation of various products. The energies of the stationary points were obtained at the CCSD(T)/cc-pVTZ//M06-2X/6-311++G(3df,3pd) level of theory. The symbol RC*n* (*n* = 2, 4, 5) refers to prereactive complexes, TS*n* (*n* = 13–16) refers to TSs, and PC*n* (*n* = 13–15) refers to postreactive complexes.

attached to the sulfinyl ($-S(=O)$) moiety of DPTS. The energies displayed on the PESs were calculated at the CCSD(T)/cc-pVTZ//M06-2X/6-311++G(3df,3pd) level of theory. Each hydrogen abstraction channel starts initially by forming a barrier-less prereactive complex (RC1 and RC2) with binding energies of −7.5 and −4.4 kcal mol^{-1} below those of the separated reactants (see Figure 2), respectively. These prereactive complexes are stabilized by the formation of

https://dx.doi.org/10.1021/acs.jpca.0c05200
J. Phys. Chem. A 2020, 124, 8292–8304

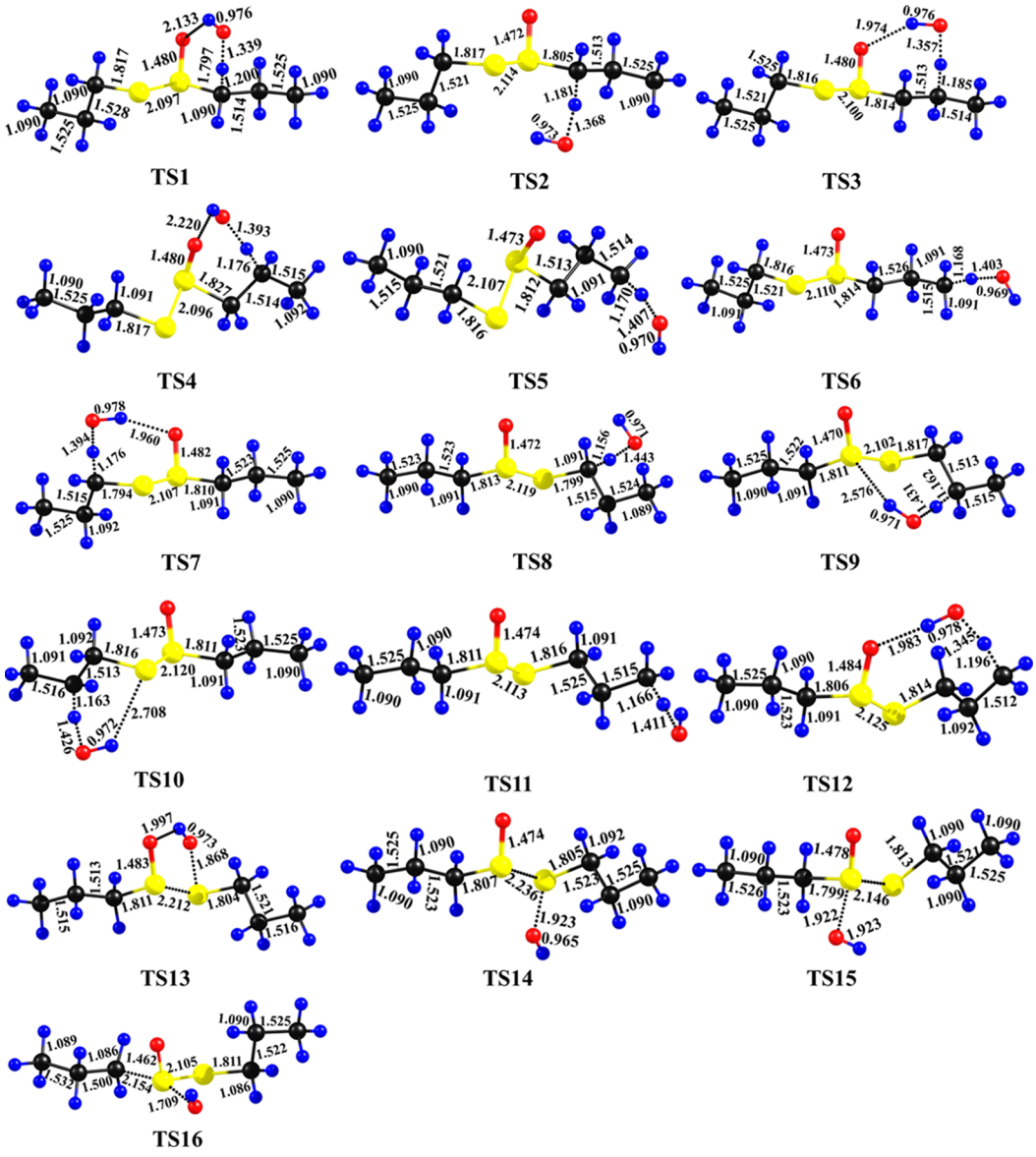

Figure 5. Optimized geometries of all TSs for the DPTS + •OH reaction obtained at the M06-2X/6-311++G(3df,3pd) level of theory. The black, yellow, red, and blue colors denote carbon, sulfur, oxygen, and hydrogen atoms, respectively.

hydrogen bonding interactions (see Figure S1). After the formation of RC1, each H atom abstraction path proceeds through the formation of various TSs to form the corresponding products. For example, TS1, TS3, TS4, TS5, and TS6 are formed via a prereactive complex (RC1), and TS2 is formed via RC2. All the TSs lead to the formation of the corresponding bimolecular products via their corresponding product complexes. TS1, TS3, TS4, TS5, and TS6 form from RC1 through the approach of the O− atom of •OH toward an H− atom of the $-CH_2$ or $-CH_3$ moieties of the DPTS propyl groups in such a way that abstraction of an H-atom occurs via formation of a ring-like TS, with corresponding barrier heights of −1.9, −2.1, 0.0, 3.2, and 2.5 kcal mol^{-1}, respectively. These TSs proceed further to form the corresponding product complexes (PC1, PC3, PC4, PC5, and PC6), which leads to the formation of bimolecular products (X + H_2O, where X = P1, P2, P3), as shown in Figure 2. The other TS (TS2) forms between the prereactive complex (RC2) and postreactive complex (PC2), with a barrier height of 1.0 kcal mol^{-1} above that of the separated reactants. This reaction then proceeds further by unimolecular decomposition of PC2 to form the products P1 + H_2O, as shown in Figure 2. The presented results suggest that the abstraction of an H atom from the middle $-CH_2$ group of the propyl moiety that is attached to the sulfinyl (−S(=O)) of DPTS (via TS3), leading to formation of P2 + H_2O as products, is more dominant.

The PESs for the H atom abstraction pathways associated with the second propyl group (i.e. the one attached to the −S− atom of DPTS), and mediated by •OH, are shown in Figure 3. The potential energy profiles begin with formation of prereactive complex RC3, with a binding energy of ∼7.0 kcal mol^{-1} below the energy of the starting reactants. In RC3, the hydrogen-bonded O-atom of •OH approaches the H− atoms of the two $-CH_2$ and $-CH_3$ moieties of the propyl group, and can abstract each H atom via TS7, TS8, TS9, TS10, TS11, and TS12, with barrier heights of −3.9, 1.3, 1.3, 0.4, 3.3, and −0.2 kcal mol^{-1}, relative to the DPTS + •OH separated reactants, respectively. These six TSs proceed to the stable postreactive

https://dx.doi.org/10.1021/acs.jpca.0c05200
J. Phys. Chem. A 2020, 124, 8292−8304

complexes PC7, PC8, PC9, PC10, PC11, and PC12 and then to form their corresponding bimolecular products (Y + H_2O, where Y = P4, P5, P6). The energies of TS7−TS12 suggest that abstraction of a hydrogen from the $-CH_2$ that is attached to the −S− atom of DPTS (via TS7) is more dominant compared to the other possible pathways. Overall, based on the barrier heights for all the possible hydrogen atom abstraction paths, the formation of TS7 was identified to be the most dominant.

While DMTS and DPTS are congeners which each contain two methyl groups, the outcomes for their interactions with •OH differ. Because they are both asymmetrical thiosulfinates, the pair of methyl groups that they each have are nonidentical. In the DPTS + •OH reaction, two H-abstraction TSs were found for each methyl group, leading to a total of four H-abstraction TSs. On the other hand, for the DMTS + •OH reaction system, three different H-abstraction TSs from the $-CH_3$ group attached to the −S(=O) moiety, and two different H-abstraction TSs from the $-CH_3$ group attached to the S-atom, lead to a total of five H-abstraction TSs.[13] The barrier heights for the H-abstraction from the $-CH_3$ group of the propyl moiety attached to the sulfinyl group in DPTS were found to be 2.5 and 3.2 kcal mol^{-1}, and the barrier heights for the same reaction for the $-CH_3$ group of DMTS were reported[13] to be 0.7, 1.9, and 2.7 kcal mol^{-1}, respectively. Similarly, the barrier heights for the H-abstraction from the $-CH_3$ moiety of the propyl group attached to the S-atom of DPTS were calculated to be −0.2 and 3.3 kcal mol^{-1}, while the values for the same reaction in the case of DMTS were reported to be −0.4 and 1.7 kcal mol^{-1}.[13] The lower barrier height values for the H-abstraction reactions in the DMTS + •OH reaction are likely because of two main reasons: (1) the presence of H-bonding interactions between the H-atom of the •OH and the O-atom and S-atom of DMTS, leading to greater stabilization of the TSs when compared to the analogous H-abstraction TSs in the DPTS + •OH reactions which do not exhibit these hydrogen bonding interactions, and (2) the DPTS + •OH reaction energy calculations reported here were performed at the CCSD(T)/cc-pVTZ//M06-2X/6-311++G-(3df,3pd) level, whereas the DMTS + •OH reaction energies were conducted at the CCSD(T)/aug-cc-pVTZ//M06-2X/6-311++G(3df,3pd) level.

The second class of possible DPTS + •OH reactions involve substitution pathways. The PESs for these channels are illustrated in Figure 4. As shown, the addition of •OH above the plane of the −S− atom, followed by −S(=O)−S single bond cleavage, proceeds via RC4 to furnish TS13 with a barrier height of 1.6 kcal $mole^{-1}$ relative to that of the separated reactants. This reaction channel then proceeds through PC13 to form bimolecular products (P7 + P8). Similarly, OH radical addition below the plane of the −S− atom of DPTS, via RC2, leads to formation of TS14, with a barrier height of −1.9 kcal mol^{-1} below that of the separated reactants. This then proceeds through the same PC13 to form P7 + P8 as final products. Two other important reactions include addition of •OH to the sulfinyl (−S(=O)) sulfur atom followed by either −S(=O)−S or −S(=O)−CH_2− single bond cleavage to generate TS15 and TS16 (via RC5), with barrier heights, respectively, of −5.4 and −3.1 kcal mol^{-1} relative to those of the DPTS + •OH separated reactants. These two pathways then proceed through formation of their corresponding postreactive complexes PC14 and PC15 to form products (P9 + P10) and (P11 + P12), respectively. Taken together, the barrier heights of all possible DPTS + •OH abstraction and substitution channels suggest that addition of •OH to the sulfinyl (−S(=O)) sulfur, followed by simultaneous cleavage of the (−S(=O)−S) single bond through TS15 (with a barrier height of −5.4 kcal mol^{-1}), is more dominant.

3.2. Theoretical Kinetic Analysis. Master Equation Solver for Multi-Energy well Reactions (MESMER (v.5.2)) kinetic code[17] was used to perform the rate coefficient calculations for DPTS + •OH reaction pathways in the form of the energy-grained master equation (EGME). This approach has been described in detail in our previous work[13] and in several other studies.[21,30,31] It considers the reaction dynamics as influenced by molecular collisions because of energy dissipative processes and provides the kinetics of the reaction system at the microcanonical level. The microcanonical rate coefficients are acquired from RRKM theory, and the energy transfer properties for all the potential wells or intermediates are calculated assuming an exponential-down model represented by the average energy transferred upon collision with the bath gas (ΔE_{down}). The required input parameters (energies, vibrational frequencies, and rotational constants) in the MESMER calculations for all the stationary points on the PESs (eqs 6−14, and Figures 2−4) were obtained from *ab initio*/DFT electronic structure calculations performed at the CCSD(T)/cc-pVTZ//M06-2X/6-311++G-(3df,3pd) level. Rate coefficients were extracted from the chemically significant eigenvalues using a procedure similar to that described by Bartis and Widom.[32−35] MESMER solves the master equation and the subsequent eigenvalue−eigenvector analysis and outputs the concentration time-profile for each species together, with the phenomenological rate coefficients of the system.

The PESs shown in Figures 2−4 suggest that the association of the reactants (DPTS and •OH) in the entrance channels leads to formation of prereactive complexes (RCs), which then form corresponding postreactive complexes (PCs) via a TS. The formed PCs dissociate into individual products, which is clearly seen from the exit channels of all the PESs (see Figures 2−4). The association of starting reactants and the reverse of the dissociation of products in the PESs were found to be barrier-less processes. To calculate the microcanonical rate coefficients for these kinds of reactions, MESMER uses the inverse laplace transform (ILT) approach.[17] Such barrier-less reactions have rate coefficients that are close to the capture limit (i.e. $\sim 1 \times 10^{-10}$ cm^3 $molecule^{-1}$ s^{-1}). In the present work, the Arrhenius pre-exponential factor (A) that was used in the ILT approach was set to values between 5.0×10^{-10} and 1.0×10^{-11} cm^3 $molecule^{-1}$ s^{-1} for the entrance and exit channels of the DPTS + •OH reaction, respectively. The other required parameters of activation energy and the modified Arrhenius parameter were set to 0 kcal mol^{-1} and 0.1, respectively. MESMER uses the RRKM theory to calculate microcanonical rate coefficients for the reaction steps involving RCs to PCs through a well-defined TS.

3.3. Kinetics. Rate coefficients for all the reaction pathways for the DPTS + •OH system were calculated using the MESMER kinetic code in the temperature range of 200−300 K and at 1 atm pressure.[17] As described in the theoretical kinetic analysis section, the necessary input parameters for the MESMER calculations were taken from the present computational calculations. Lennard-Jones (L-J) parameters are also required for the potential wells (RCs and PCs) involved in the

https://dx.doi.org/10.1021/acs.jpca.0c05200
J. Phys. Chem. A 2020, 124, 8292−8304

PESs and for the bath gas (N_2 gas) in the MESMER rate calculations. The RCs and PCs involved in all the PESs of the DPTS + •OH reaction system are similar in size to *n*-octane. Therefore, we used its L-J parameter values of σ = 6.3 Å and ε = 828.2 K in the rate calculations.[36] The L-J parameters for the N_2 bath gas (i.e. σ = 3.9 Å and ε = 48 K) were obtained from the literature.[17] The average energy transfer in the downward direction that was used in the exponential down collision energy transfer model for the DPTS + •OH reaction pathways was set to $\langle \Delta E_d \rangle$ = 200 cm^{-1}. The selected value is based on similar studies of •OH reactions with other compounds.[13,37] Variations of $\langle \Delta E_d \rangle$ of between 100 and 300 cm^{-1} resulted in changes in the rate coefficients within the studied temperature range of <2%.

As discussed in the theoretical kinetic analysis section, MESMER uses the ILT method for the association and the reverse of the dissociation steps, and the RRKM theory for unimolecular reactions with well-defined TSs on the PESs. The present rate calculations also applied the Eckart tunneling correction to obtain the tunneling contribution to the reaction rate coefficients.[38] The concentration of DPTS is assumed to be in large excess because the •OH concentrations are smaller by several orders of magnitude in the atmosphere. Therefore, we considered these reaction pathways under pseudo-first-order conditions. The bimolecular rate coefficients were calculated in the atmospherically relevant temperatures between 200 and 300 K and at 1 atm for the reaction pathways that proceeded via TS1-TS16 and are displayed in Table 1. The rate coefficient values (k_{TS1} − k_{TS12}) given in Table 1 are for the H-abstraction reactions involved in the DPTS + •OH system. Although there are 12 possible H-abstraction sites in DPTS, H-abstraction from the $-CH_2$ of the propyl group attached to the S-atom of DPTS via TS7 is the only channel that effectively contributes to the total reaction. The H-abstraction rate coefficient values (k_{TS7}) via TS7 were found to be ∼1−5 orders of magnitude higher than those for the other possible H-abstraction rate coefficient values in the temperatures between 200 and 300 K. For example, the rate coefficient value for the H-abstraction reaction via TS7 at 300 K was found to be 5.75 × 10^{-11} cm^3 $molecule^{-1}$ s^{-1}, and via TS1, TS2, TS3, TS4, TS5, TS6, TS8, TS9, TS10, TS11, and TS12 were found to be 3.57 × 10^{-12}, 1.36 × 10^{-13}, 3.19 × 10^{-12}, 9.43 × 10^{-14}, 7.10 × 10^{-15}, 1.97 × 10^{-14}, 1.91 × 10^{-13}, 2.22 × 10^{-14}, 1.89 × 10^{-13}, 6.00 × 10^{-15}, and 1.33 × 10^{-13} cm^3 $molecule^{-1}$ s^{-1}, respectively.

To see the competition between H-abstraction and substitution reactions involving in DPTS + •OH system more clearly, the total abstraction rate coefficients (k_{total}^{abs}) and total substitution rate coefficients (k_{total}^{sub}) were calculated by adding the individual rate coefficients for the each reaction pathway involving both H-abstraction and substitution channels (i.e. eqs 15 and 16) as follows

$$k_{total}^{abs} = k_{TS1} + k_{TS2} + k_{TS3} + k_{TS4} + 2k_{TS5} + k_{TS6} + k_{TS7} + k_{TS8} + k_{TS9} + k_{TS10} + 2k_{TS11} + k_{TS12} \quad (15)$$

$$k_{total}^{sub} = k_{TS13} + k_{TS14} + k_{TS15} + k_{TS16} \quad (16)$$

In the above equations, k_{TSn} (n = 1−16) represents the corresponding H-abstraction and substitution reaction rate coefficients. The calculated total H-abstraction rate coefficient (k_{total}^{abs}) and total substitution rate coefficient (k_{total}^{sub}) in the temperature range between 200 and 300 K are given in Table

Table 1. Calculated Bimolecular Rate Coefficients (in cm^3 $molecule^{-1}$ s^{-1}) for all the Possible Abstraction and Substitution Pathways Involved in the DPTS + •OH Reaction in the Temperatures Between 200 and 300 K and at 1 atm Pressure

T	k_{TS1}	k_{TS2}	k_{TS3}	k_{TS4}	$2k_{TS5}$	k_{TS6}	k_{TS7}	k_{TS8}	k_{TS9}
200	4.95 × 10^{-12}	2.06 × 10^{-13}	3.85 × 10^{-12}	1.50 × 10^{-13}	6.40 × 10^{-16}	2.15 × 10^{-15}	2.26 × 10^{-10}	6.12 × 10^{-14}	1.09 × 10^{-14}
220	4.88 × 10^{-12}	1.73 × 10^{-13}	4.14 × 10^{-12}	1.41 × 10^{-13}	1.28 × 10^{-15}	4.17 × 10^{-15}	1.75 × 10^{-10}	8.52 × 10^{-14}	1.37 × 10^{-14}
240	4.74 × 10^{-12}	1.54 × 10^{-13}	4.11 × 10^{-12}	1.29 × 10^{-13}	2.22 × 10^{-15}	6.98 × 10^{-15}	1.33 × 10^{-10}	1.11 × 10^{-13}	1.61 × 10^{-14}
250	4.58 × 10^{-12}	1.48 × 10^{-13}	4.02 × 10^{-12}	1.21 × 10^{-13}	2.82 × 10^{-15}	8.67 × 10^{-15}	1.61 × 10^{-10}	1.22 × 10^{-13}	1.71 × 10^{-14}
260	4.39 × 10^{-12}	1.43 × 10^{-13}	3.89 × 10^{-12}	1.15 × 10^{-13}	3.50 × 10^{-15}	1.05 × 10^{-14}	1.00 × 10^{-10}	1.36 × 10^{-13}	1.81 × 10^{-14}
280	3.98 × 10^{-12}	1.38 × 10^{-13}	3.54 × 10^{-12}	1.03 × 10^{-13}	5.12 × 10^{-15}	1.47 × 10^{-14}	7.61 × 10^{-11}	1.63 × 10^{-13}	2.01 × 10^{-14}
300	3.57 × 10^{-12}	1.36 × 10^{-13}	3.19 × 10^{-12}	9.43 × 10^{-14}	7.10 × 10^{-15}	1.97 × 10^{-14}	5.75 × 10^{-11}	1.91 × 10^{-13}	2.22 × 10^{-14}

k_{TS10}	$2k_{TS11}$	k_{TS12}	k_{TS13}	k_{TS14}	k_{TS15}	k_{TS16}	k_{total}^{abs}	$k_{total}^{abs+sub}$
1.30 × 10^{-13}	7.26 × 10^{-16}	2.96 × 10^{-13}	1.05 × 10^{-15}	1.89 × 10^{-12}	9.07 × 10^{-10}	5.16 × 10^{-12}	2.36 × 10^{-10}	9.14 × 10^{-10}	1.15 × 10^{-9}
1.54 × 10^{-13}	1.24 × 10^{-15}	2.70 × 10^{-13}	1.66 × 10^{-15}	1.43 × 10^{-12}	5.70 × 10^{-10}	4.60 × 10^{-12}	1.85 × 10^{-10}	5.76 × 10^{-10}	7.61 × 10^{-10}
1.69 × 10^{-13}	1.96 × 10^{-15}	2.31 × 10^{-13}	2.31 × 10^{-15}	1.11 × 10^{-12}	3.59 × 10^{-10}	3.95 × 10^{-12}	1.43 × 10^{-10}	3.64 × 10^{-10}	5.07 × 10^{-10}
1.74 × 10^{-13}	2.42 × 10^{-15}	2.11 × 10^{-13}	2.64 × 10^{-15}	9.87 × 10^{-13}	2.86 × 10^{-10}	3.63 × 10^{-12}	1.70 × 10^{-10}	2.91 × 10^{-10}	4.61 × 10^{-10}
1.77 × 10^{-13}	2.96 × 10^{-15}	1.92 × 10^{-13}	2.97 × 10^{-15}	8.88 × 10^{-13}	2.29 × 10^{-10}	3.33 × 10^{-12}	1.09 × 10^{-10}	2.33 × 10^{-10}	3.42 × 10^{-10}
1.84 × 10^{-13}	4.28 × 10^{-15}	1.59 × 10^{-13}	3.61 × 10^{-15}	7.11 × 10^{-13}	1.47 × 10^{-10}	2.80 × 10^{-12}	8.44 × 10^{-11}	1.51 × 10^{-10}	2.35 × 10^{-10}
1.89 × 10^{-13}	6.00 × 10^{-15}	1.33 × 10^{-13}	4.24 × 10^{-15}	5.86 × 10^{-13}	9.68 × 10^{-11}	2.35 × 10^{-12}	6.51 × 10^{-11}	9.97 × 10^{-11}	1.65 × 10^{-10}

https://dx.doi.org/10.1021/acs.jpca.0c05200
J. Phys. Chem. A 2020, 124, 8292−8304

1. The data from the table clearly suggest that the total H-abstraction reaction rate coefficient values are ∼2−4 times smaller than the total substitution reaction rate coefficient values in the studied temperature range. Therefore, the substitution reactions are more dominant than the H-abstraction reactions.

The data from Table 1 suggest that the rate coefficient obtained via TS15 is higher than those for the other possible abstraction and substitution paths in the studied temperature range. Therefore, it can be concluded that addition of •OH to the sulfinyl moiety of DPTS, followed by S(=O)−S single-bond cleavage through TS15, leading to the formation of propanethiyl radical (PTR) and propanesulfinic acid as products, is a major pathway when compared to the other possible channels. For example, the bimolecular rate coefficient at 300 K via TS15 for the DPTS + •OH reaction pathway was found to be 9.7×10^{-11} cm^3 molecule^{-1} s^{-1}, whereas all the other reaction channels, with the exception of the abstraction channel via TS7 with a rate coefficient of 5.8×10^{-11} cm^3 molecule^{-1} s^{-1} at the same temperature, were ∼1−5 orders of magnitude smaller. Furthermore, the Eckart tunneling[38] contributions to the rate coefficients for each reaction path were also estimated. These values, which are listed in Table S7, indicate that the abstraction channel rate coefficients increased by ∼2−6 times, and that the values for the substitution channels are almost independent of tunneling in the studied temperature range. This situation is clearly due to the observation that the M06-2X calculated imaginary frequencies for the TSs involved in the substitution channels are less than 600 cm^{-1} (see Table S5). Hence, they have a negligible influence on the calculated rate coefficients.[37]

The total rate coefficients ($k_{\text{total}}^{\text{DPTS+OH}}$) for the DPTS + •OH reaction were calculated by summing the individual reaction path rate coefficients at the corresponding temperatures using eq 17, where $k_{\text{total}}^{\text{DPTS+OH}}$ is the total rate coefficient for the reaction of DPTS + •OH, and $k_{\text{TS}n}$ (n = 1−16) represents the individual reaction path rate coefficients via TS1−TS16. In the total rate coefficient calculations, the contributions of rate coefficients for the reactions proceeding via TS5 and TS11 were multiplied by a factor of 2 (see eq 17). This is because the TS energy for the abstraction of two hydrogen atoms from the two methyl groups of DPTS involves the same energy, and hence, they were considered as a single TS.

$$k_{\text{total}}^{\text{DPTS+OH}} = k_{\text{TS1}} + k_{\text{TS2}} + k_{\text{TS3}} + k_{\text{TS4}} + 2k_{\text{TS5}} + k_{\text{TS6}} + k_{\text{TS7}} + k_{\text{TS8}} + k_{\text{TS9}} + k_{\text{TS10}} + 2k_{\text{TS11}} + k_{\text{TS12}} + k_{\text{TS13}} + k_{\text{TS14}} + k_{\text{TS15}} + k_{\text{TS16}} \quad (17)$$

The calculated total rate coefficients are provided in Table 1, and the values are also plotted in Figure 6 for the temperatures between 200 and 300 K at a pressure of 1 atm. The total rate coefficients and the trend in Figure 6 revealed a negative temperature dependence within the entire studied temperature range. There are no reported studies available on the DPTS + •OH reaction using both experimental and theoretical calculations with which to compare our calculated rate coefficient values. Therefore, we compared the rate coefficients calculated for the DPTS + •OH reaction in the temperatures between 200 and 300 K with those computed for the reaction of DMTS + •OH within the same temperature range, and these are plotted in Figure 6. The rate coefficients for the

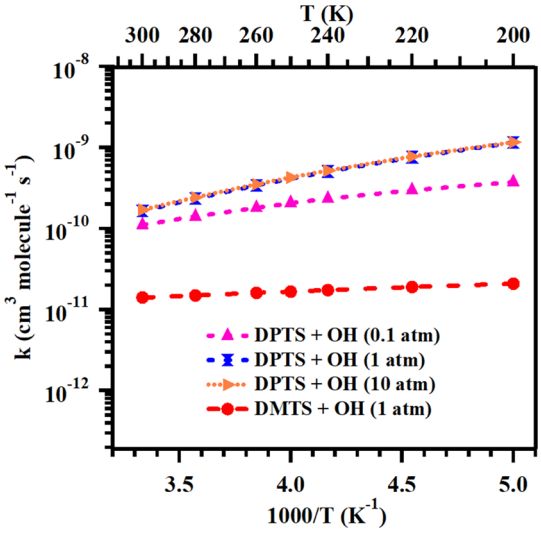

Figure 6. Comparison of the calculated total rate coefficients for the reaction of DPTS with •OH to form various products over the temperature range 200−300 K and at pressures of 0.1, 1, and 10 atm. The total rate coefficients for the reaction of dimethyl thiosulfinate (DMTS) with •OH reported over the same temperature range and at 1 atm pressure (red colored circles) are included for comparison.

DPTS + •OH reaction were found to be 10 to 55 times higher than those for the DMTS + •OH reaction in the studied temperature range (see Figure 6). For example, the rate coefficient for the DPTS + •OH reaction at 300 K was $k_{\text{total}}^{\text{DPTS+OH}} = 1.7 \times 10^{-10}$ cm^3 molecule^{-1} s^{-1} and that for the DMTS + •OH reaction was k_{total} (CH_3−S(O)S−CH_3 + •OH) $= 1.4 \times 10^{-11}$ cm^3 molecule^{-1} s^{-1}. This suggests that the DPTS + •OH reaction rate coefficient is ∼10 times higher than the value for the DMTS + •OH reaction.[13] This result can be ascribed to the lower barrier heights for the abstraction channels and the increase in the number of H-abstraction sites for the DPTS + •OH reaction when compared to the DMTS + •OH reaction.

We also compared the total H-abstraction reaction rate coefficients involved in DMTS + •OH and DPTS + •OH reactions. At 300 K, the total H-abstraction rate coefficient for DMTS + •OH is reported to be 2.43×10^{-12} cm^3 molecule^{-1} s^{-1}, which is ∼27 times smaller than the analogous reaction in the DPTS + •OH system at the same temperature. The total abstraction rate coefficients for the DPTS + •OH reaction are higher, even though the barrier heights for the −CH_3 group H-abstraction reactions involving the DMTS + •OH reaction system are lower than the barrier height values of the same reactions involving DPTS + •OH. This is mainly because of the presence of four different −CH_2 group H-abstraction reactions of the DPTS, which contribute to the total H-abstraction reaction rate coefficient involved in the DPTS + •OH reaction system.

We performed rate coefficient calculations for all the pathways using the MESMER kinetic code in the temperatures between 200 and 300 K and the pressures used were 0.1, 1, and 10 atm. The corresponding values are displayed in Tables 1, S8, and S9 of the Supporting Information. The values in Tables 1, S8, and S9 suggest that the individual H-abstraction reaction paths rate coefficients (k_{TS1} − k_{TS12}) show a weak pressure dependence at lower temperatures (<250 K). Beyond this temperature, rate coefficient values were found to be

https://dx.doi.org/10.1021/acs.jpca.0c05200
J. Phys. Chem. A 2020, 124, 8292−8304

independent of pressure. The total rate coefficients were obtained by adding the individual reaction channel rate coefficients obtained at 0.1, 1, and 10 atm in the same temperature range. The results are also displayed in Tables 1, S8, and S9, and the values are plotted in Figure 6. The total rate coefficients curves at 1 and 10 atm nearly overlap for the DPTS + •OH reaction. At 0.1 atm, the total rate coefficients show little pressure dependence at low temperatures (<250 K) and beyond this temperature, rate coefficient values are nearly independent of pressure. For example, at 300 K, the total DPTS + •OH reaction rate coefficients at pressures 0.1, 1, and 10 atm were found to be 1.11×10^{-10}, 1.65×10^{-10}, and 1.71×10^{-10} cm^3 molecule^{-1} s^{-1}, respectively.

The reaction for the major substitution channel (R12) most likely follows a two-step mechanism. The reaction first proceeds via the association of •OH with DPTS to form a prereactive complex (RC5) with simultaneous cleavage of the S(=O)−S single bond via TS15, leading to the formation of propanesulfinic acid and PTR. To verify that this reaction most likely proceeds via a prereactive or adduct formation mechanism, we performed rate coefficient calculations for the association reaction step (DPTS + •OH → RC5) using the Bartis and Widom method at 240 K, within a pressure range from 10^{-5} to 10^{9} atm. The results are presented in the Troe-type plot shown in Figure S2. The resultant rate coefficient trend shows the standard pressure-dependent form for the association reaction,[39] and the values increase to a high-pressure limit. Therefore, we can conclude that the present reaction proceeds in two steps (i.e. DPTS + •OH undergoes association to form a prereactive complex, and then cleavage of the S(=O)−S single bond leads to the formation of products such as propanesulfinic acid and PTR).

Branching ratios were calculated to determine the contribution from each reaction path to the total rate coefficient in the studied temperature range of 200−300 K. The branching ratio values of all the reaction pathways via the various TSs (TS1−TS16) are displayed in Table S10. Each of the reaction path contributions shown were calculated from the ratio of individual channel rate coefficients, to the sum of the rate coefficients of all the channels at the corresponding temperatures. The results, which are presented in Table S10, suggest that the substitution channel proceeding through TS15 is kinetically the more dominant reaction. The branching ratio contribution of this reaction to the total reaction was found to decrease from 79 to ∼59% as the temperature increased from 200 to 300 K. However, the contribution of the abstraction reaction via TS7 was found to increase with increasing temperature (from 20 to 35%) for the total reaction in the studied temperature range. The other remaining reaction contributions were found to be ∼1 to 5 orders of magnitude smaller compared to the values of the reactions that proceeded through TS7 and TS15. For example, the branching ratio values (in percent) for all the possible reaction paths at 300 K were estimated to be: TS1 = 2.2%, TS2 = 0.08%, TS3 = 1.9%, TS4 = 0.06%, TS5 = 4.3×10^{-3}%, TS6 = 1.2×10^{-2}%, TS7 = 34.9%, TS8 = 0.1%, TS9 = 0.01%, TS10 = 0.12%, TS11 = 3.6×10^{-3}%, TS12 = 0.08%, TS13 = 2.6×10^{-3}%, TS14 = 0.4%, TS15 = 58.7%, and TS16 = 1.4%. The calculated total hydrogen abstraction rate coefficient ($k_{\text{total}}^{\text{abs}}$) and total substitution rate coefficient ($k_{\text{total}}^{\text{sub}}$) in the temperature range between 200 and 300 K are given in Table 1. The data from Table 1 reveal that the total contribution of hydrogen abstraction reactions is ∼20−40%, and the remaining contribution of ∼60−80% is from the substitution channels in the studied temperatures between 200 and 300 K.

In addition, we also estimated the atmospheric lifetime[13,28] of DPTS due to its reaction with tropospheric •OH using eq 18

$$\tau = 1/k_{\text{OH}}[\text{OH}] \tag{18}$$

where k_{OH} represents the total rate coefficient (in cm^3 molecule^{-1} s^{-1}) for the DPTS + •OH reaction, and [OH] is the average tropospheric concentration[40] of the OH radical (∼1.0×10^6 molecules cm^3). Using our calculated DPTS + •OH reaction rate coefficients, the atmospheric lifetime of DPTS was determined to be 0.3−1.7 h in the studied temperature between 200 and 300 K. Therefore, the contribution of DPTS to global warming is negligible because its lifetime in the atmosphere is very short (less than 2 h).

Global warming potential (GWP) provides a relative measure of the heat trapped by a greenhouse gas in the atmosphere. It can be estimated using time-integrated radiative forcing of the atmospheric gas relative to carbon dioxide. This is an important atmospheric parameter which can be estimated for the reactant and various products present in the DPTS + •OH reaction system using eq 19

$$\text{GWP} = \frac{a\int_0^t e^{-t/\tau}\, d\tau}{\text{AGWP}_{\text{CO}_2}} \tag{19}$$

where a is the total radiative forcing (W m^{-2} ppbv^{-1}), t is the time horizon, and $\text{AGWP}_{\text{CO}_2}$ is the absolute GWP for CO_2. The equation provided by Pinnock et al.[41] was utilized in the calculation of the total radiative forcing (a), and it can be calculated by using eq 20 given below

$$a = \sum_k A_k F(\nu_k) \tag{20}$$

In eq 20, A_k represents the absorption cross section (cm^3 molecule^{-1}) and $F(\nu_k)$ represents the radiative forcing function per unit cross section per wave number in (W m^{-2} (cm^{-1}))$^{-1}$ (cm^2 molecule^{-1})$^{-1}$). The vibrational frequencies (ν_k) and intensities (A_k) of the corresponding vibrational mode k for the DPTS reactant, and the various products present in the DPTS + •OH reaction system, were taken from our computational calculations. The atmospheric lifetime (τ) of DPTS with respect to •OH was obtained from the present study. Rate coefficients were not available in the literature for products such as propanesulfinic acid and propanethial with •OH reactions to estimate their atmospheric lifetimes, which is required in calculating the GWP. Therefore, to get the atmospheric lifetimes of the products, the rate coefficients were estimated using the Atmospheric Oxidation Program for Microsoft Windows (AOPWIN v.1.92).[42] By this method, the bimolecular rate coefficients at 298 K for the propanesulfinic acid + •OH and propanethial + •OH were estimated to be 1.04×10^{-11} and 1.99×10^{-11} cm^3 molecule^{-1} s^{-1}, respectively. Using the rate coefficient data, the atmospheric lifetime of the propanesulfinic acid and propanethial with respect to •OH were estimated, and the values are given in Table 2. The atmospheric lifetime for SO_2 was calculated using the rate coefficient[43] reported for the reaction SO_2 + •OH at 298 K and was found to be 1.25×10^{-12} cm^3 molecule^{-1} s^{-1}. The calculated GWPs for the different horizons of time for the reactant (DPTS) and three different products (propanesulfinic

https://dx.doi.org/10.1021/acs.jpca.0c05200
J. Phys. Chem. A 2020, 124, 8292−8304

Table 2. Calculated Atmospheric Lifetimes and GWPs of DPTS, Propanesulfinic Acid, Propanethial, and Sulfur Dioxide

molecule	lifetime (days)	GWP		
		20	50	100
DPTS	0.07	0.02	0.009	0.005
propanesulfinic acid	1.11	1.00	0.44	0.26
propanethial	0.58	0.14	0.06	0.03
sulfur dioxide	9.26	1.76	0.78	0.45

acid, propanethial, and SO_2) are given in Table 2. The GWP of DPTS is almost 2 orders of magnitude smaller compared to the products (see Table 2). Therefore, the degradation products may have a higher impact on global warming as compared to the DPTS reactant from which they were derived.

A mechanism analogous to that for the DMTS + •OH reaction was also considered for the atmospheric oxidation of DPTS initiated by •Cl radical. The most plausible mechanism proposed for the DPTS + •Cl reaction is shown in Figure 7. Like the DMTS + •OH reaction mechanism, the DPTS + •Cl reaction also undergoes hydrogen abstraction and substitution pathways (Figure 7). All of the possible hydrogen abstraction channels for the DPTS by •Cl system lead to formation of C-atom-centered DPTS radicals with HCl as products. Presented in Figure 7 are three substitution pathways available for the DPTS + •Cl reaction: (i) •Cl attack above or below the S-atom of DPTS, followed by S(=O)−S single bond fission via substitution pathway 1, leading to formation of propylsulfinyl radical [$CH_3CH_2CH_2S^{\bullet}(=O)$] and propylsulfenyl chloride ($CH_3CH_2CH_2S-Cl$) as products and (ii) substitution pathways 2 and 3 in which attack by •Cl on the S-atom of the S(=O) moiety is followed by either C−S(=O) or S−S(=O) single bond cleavage, leading to formation of $CH_3CH_2CH_2S-S(=O)-Cl$ + propyl ($CH_3CH_2C{\cdot}H_2$) radical or 1-propanesulfinyl chloride ($CH_3CH_2CH_2S(=O)-Cl$) + propanethiyl ($CH_3CH_2CH_2S^{\bullet}$) radical as products. Thus, the mechanism suggests formation of compounds such as $CH_3CH_2CH_2S-Cl$, $CH_3CH_2CH_2S-S(=O)-Cl$, $CH_3CH_2CH_2S(=O)-Cl$, and HCl as final products. Further studies are required to estimate the atmospheric fate and lifetime of DPTS with •Cl and the corresponding chlorinated products. Because chlorinated compounds generally have longer lifetimes and can diffuse into the stratosphere, they can serve as a potential source of halogen atoms that could disturb the ozone balance in the stratosphere.[44,45] Therefore, these compounds might have adverse effects on the stratospheric ozone layer.

3.4. Atmospheric Fate of PTR in the Presence of $^3O_2$.

The energetics and rate coefficient data that were determined in this work suggest that the DPTS + •OH reaction predominantly leads to the formation of PTR in the atmosphere. Once released, it can rapidly react with molecular oxygen ($^3O_2$), because atmospheric oxygen is present in large quantities in the troposphere.[21,28] Thus, we also investigated the atmospheric fate of PTR in the presence of $^3O_2$ using the same computational methods described earlier. The PES diagram involving multichannel pathways for PTR + $^3O_2$ is shown in Figure 8. The reactants, intermediates, TSs, and products on the PESs were optimized at the M06-2X/6-311++G(3df,3pd) level of theory, and the energies displayed on the PESs were computed at the CCSD(T)/cc-pVTZ//M06-2X/6-311++G(3df,3pd) level. The optimized structures of all the minima present on the PES involving all the possible pathways are shown in Figures 8 and S3. The T1 diagnostic values for

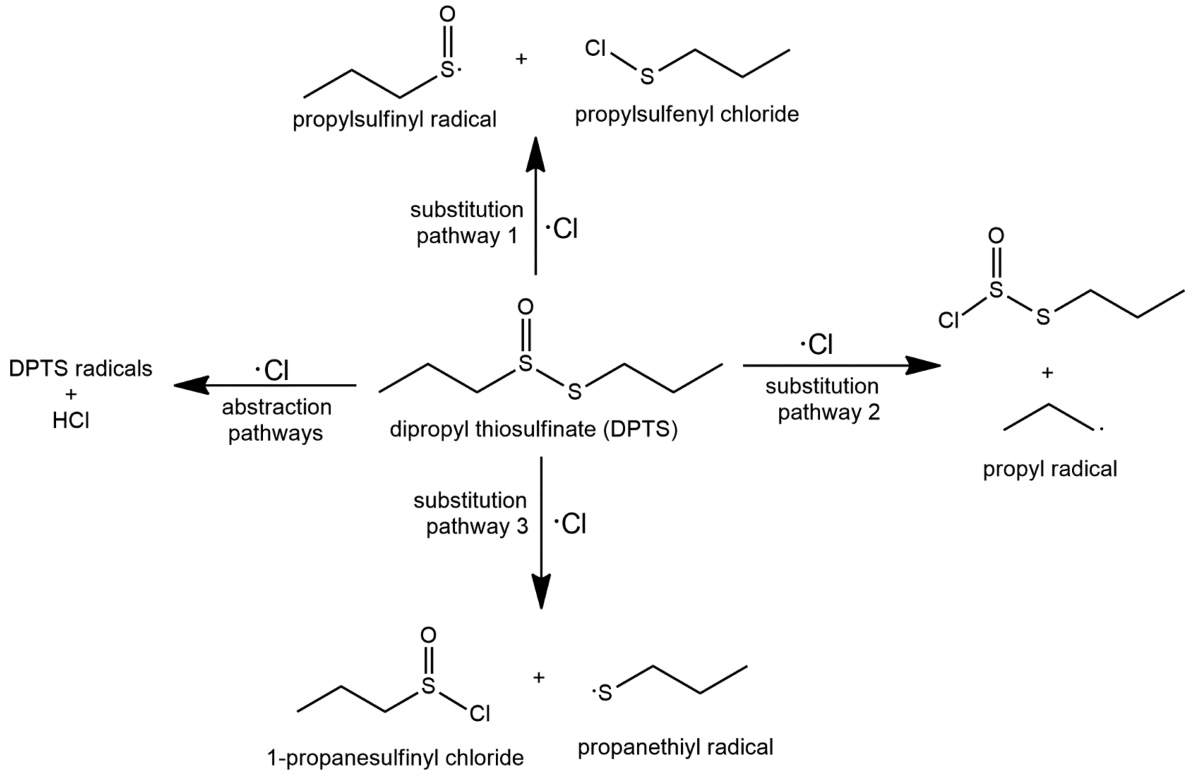

Figure 7. Most plausible mechanism for the atmospheric oxidation of DPTS initiated by Cl radicals to form various chlorinated products in the troposphere.

https://dx.doi.org/10.1021/acs.jpca.0c05200
J. Phys. Chem. A 2020, 124, 8292−8304

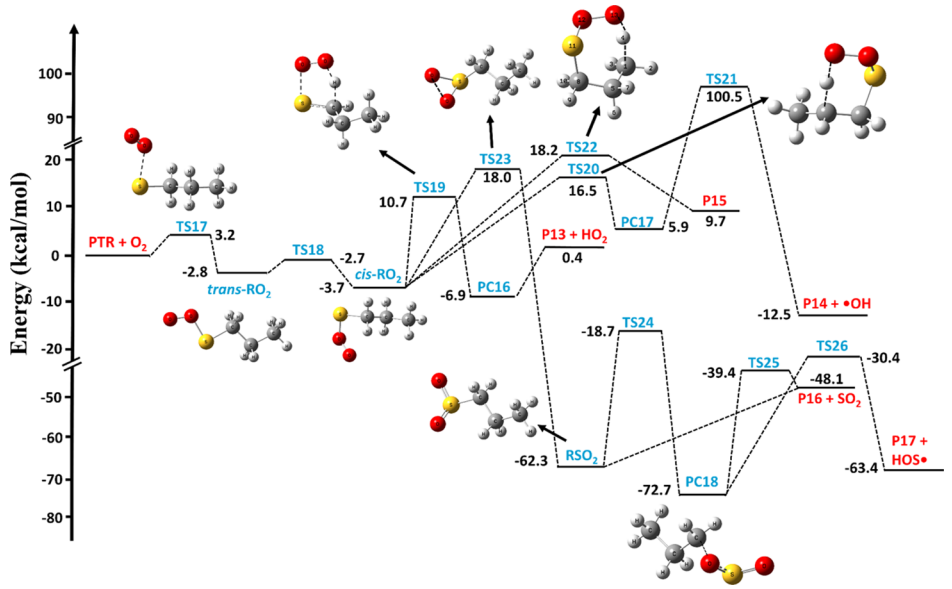

Figure 8. PES diagram for the PTR + $^3O_2$ reaction to form various products, obtained at the CCSD(T)/cc-pVTZ//M06-2X/6-311++G(3df,3pd) level of theory.

the PTR + $^3O_2$ reaction were also calculated (at the CCSD(T)/cc-pVTZ level). The T1 diagnostic values for all species were observed to be smaller than 0.03. This indicates that the multireference character of the CCSD(T) wave functions was negligible.[46] Figure 8 shows that the association of reactants (i.e. PTR and $^3O_2$) leads to an adduct (*trans*-RO_2) via TS17, with a barrier height of 3.2 kcal mol^{-1} above that of the starting PTR + O_2-separated reactants. The binding energy of the *trans*-RO_2 was computed to be 2.8 kcal mol^{-1} below that of the separated reactants at the CCSD(T)//M06-2X level. The formed *trans*-RO_2 adduct may undergo several isomerization reaction paths such as: (1) internal rotation about the R−OO single bond; (2) H-atom transfer; and (3) intramolecular rearrangement of the S−O−O moiety.

The *trans*-RO_2 primarily undergoes internal rotation about the R−OO single bond via TS18 to form *cis*-RO_2 with a barrier height of −2.7 kcal mol^{-1} relative to that of the separated reactants. The energy of *cis*-RO_2 is ∼1.0 kcal mol^{-1} more stable than the *trans*-RO_2 mostly because of the two internal hydrogen bonds between the terminal peroxy O-atom and the H-atoms of the two $-CH_2$ groups. *cis*-RO_2 can undergo decomposition through four additional forward reaction channels to form various products. One involves elimination of the HO_2 radical from *cis*-RO_2, yielding propanethial (P13). This path was found to have a lower barrier than the other three possible channels (see Figure 8), and it is therefore concluded that this reaction is the most important under atmospheric conditions. It proceeds via H-atom transfer from the $-CH_2$ moiety to the terminal peroxy O-atom, with simultaneous cleavage of the S−O single bond, and formation of a C−S double bond through a five-membered ring TS structure (TS19—Figure 8). The barrier height for this reaction via TS19 was found to be 10.7 kcal mol^{-1} above that of the PTR + O_2 separated reactants.

The second involves hydrogen atom transfer reactions of *cis*-RO_2 by two pathways: (i) transfer of the H atom of the $-CH_2$ moiety to the terminal O-atom of *cis*-RO_2 via TS20, with a barrier height of 16.5 kcal mol^{-1} relative to that of the starting reactants. This pathway then proceeds via the postreactive complex PC17 to a four-membered ring product (P14) and OH radical through TS21, with a barrier height of 100.5 kcal mol^{-1} above that of the reactants; and (ii) H atom transfer from the $-CH_3$ group of *cis*-RO_2 to the peroxy-group terminal O-atom via TS (TS22). The barrier for this reaction was found to be 18.2 kcal mol^{-1} relative to that of the separated reagents, and the reaction continues to form the product (P15). Comparison of these reaction barriers suggests that of the two, H atom transfer from the $-CH_2$ group to the terminal O-atom of *cis*-RO_2 to form ROOH radical is more energetically feasible because its reaction barrier height is ∼1.7 kcal mol^{-1} lower than that of the $-CH_3$ group H-atom transfer reaction.

The third possible decomposition pathway of *cis*-RO_2 in the forward direction was found to be intramolecular rearrangement of the S−O−O group. Attack by the peroxy radical terminal O-atom on the sulfur atom of *cis*-RO_2 results in formation of a three-membered SOO ring, which then undergoes simultaneous cleavage of the weak peroxy bond (*cis*-RO—O) via TS23 with a barrier height of 18.0 kcal mol^{-1} relative to that of the separated PTR + O_2 reactants. This results in formation of the more stable RSO_2 adduct (R = $CH_3CH_2CH_2$) which then further reacts by two pathways: (i) direct cleavage of the C−S single bond in R−SO_2 to form propyl radical (P16) + SO_2; and (ii) simultaneous cleavage of the C−S bond and formation of the C−O bond in RSO_2. This proceeds via TS24, with a barrier height of −18.7 kcal mol^{-1} relative to that of the separated reagents, to form adduct PC18 (see Figure 8). PC18 undergoes further cleavage of the C−O single bond via TS25 to form propyl radical (P16) + SO_2 as final products. The PC18 adduct also isomerizes via TS26 to form P17 + HOS$^\bullet$ as final products.

Based on the PTR + O_2 calculations presented here, the concerted elimination of HO_2 radical from the RO_2 adduct is the more dominant reaction at low-level concentrations of NO and HO_2 radicals. NO and HO_2 radicals are important trace molecules in the atmosphere, with concentrations in polluted urban areas of ∼9.0 × 10^{10} molecules cm^{-3} and ∼7.0 × 10^8 molecules cm^{-3}, respectively.[47] Therefore, RO_2 + NO and RO_2

https://dx.doi.org/10.1021/acs.jpca.0c05200
J. Phys. Chem. A 2020, 124, 8292−8304

+ HO_2 reactions will compete with unimolecular HO_2 elimination from the RO_2 adduct in the atmosphere.

4. CONCLUSIONS

A detailed theoretical investigation of the gas-phase reaction mechanism of DPTS initiated by $^{\bullet}OH$ at the CCSD(T)//M06-2X level of theory is reported for the first time. The results reveal that the most dominant reaction results in formation of PTR and propanesulfinic acid via $^{\bullet}OH$ addition to the sulfinyl S-atom, followed by S(=O)−S single-bond fission. The rate coefficients for all of the abstraction and substitution pathways were calculated using the MESMER kinetic code in the temperature range between 200 and 300 K, and the bath gas pressures were varied between 0.1 and 10 atm. The total rate coefficient for the DPTS + $^{\bullet}OH$ reaction was estimated to be $k_{total}^{DPTS+OH} = 1.7 \times 10^{-10}$ cm^3 molecule^{-1} s^{-1} at T = 300 K and P = 1 atm. The branching ratios were calculated for all possible reaction pathways. The major reaction, which resulted in formation of PTR and propanesulfinic acid contributed ∼59% to the total reaction at 300 K. The atmospheric lifetime of DPTS was estimated to be less than 2 h in the studied temperature range. This suggests that its contribution to global warming is almost negligible. In addition, the reaction of the formed PTR + $^3O_2$ was studied. The dominant path resulted in unimolecular elimination of HO_2, yielding propanethialdehyde. Overall, the atmospheric oxidation of DPTS initiated by OH radical, and in the presence of molecular oxygen, leads to the formation of propanesulfinic acid, propanethial, SO_2, hydroperoxyl radical (HO_2), HOS radical, and propyl radical as major end products. The results suggest that while DPTS itself makes a negligible contribution to global warming, the products formed as a consequence of its interaction with OH radical may make substantial contributions to global warming, acid rain, and formation of secondary organic aerosols.

■ ASSOCIATED CONTENT

Supporting Information

The Supporting Information is available free of charge at https://pubs.acs.org/doi/10.1021/acs.jpca.0c05200.

> Calculated total electronic energies including zero-point energy corrections, optimized geometries in terms of their Z-matrices, their vibrational frequencies and rotational constants, relative energies, and imaginary frequencies of various TSs at the M06-2X level of theory, rate coefficients, tunneling contributions, and branching ratios; optimized geometries of RCs, PCs, and products for DPTS + $^{\bullet}OH$, a rate coefficient plot for the DPTS + $^{\bullet}OH$ association step to form the prereactive complex (RC5), and PTR + $^3O_2$ reactions obtained at the M06-2X/6-311++G(3df,3pd) theory level (PDF)

■ AUTHOR INFORMATION

Corresponding Author

Rabi A. Musah − *Department of Chemistry, University at Albany—State University of New York, Albany, New York 12222, United States;* orcid.org/0000-0002-3135-4130; Email: rmusah@albany.edu

Author

Parandaman Arathala − *Department of Chemistry, University at Albany—State University of New York, Albany, New York 12222, United States*

Complete contact information is available at: https://pubs.acs.org/10.1021/acs.jpca.0c05200

Notes

The authors declare no competing financial interest.

■ ACKNOWLEDGMENTS

The financial support of the National Science Foundation (grant numbers 1710221 and 1310350) to R.A.M. is gratefully acknowledged. The authors also thank the High-Performance Computing Center at the University at Albany-SUNY for their support.

■ REFERENCES

(1) Charlson, R. J.; Lovelock, J. E.; Andreae, M. O.; Warren, S. G. Oceanic phytoplankton, atmospheric sulphur, cloud albedo and climate. *Nature* **1987**, *326*, 655−661.

(2) Song, G.; Bozzelli, J. W. Structures and thermochemistry of methyl ethyl sulfide and its hydroperoxides: $HOOCH_2SCH_2CH_3$, $CH_3SCH(OOH)CH_3$, $CH_3SCH_2CH_2OOH$, and radicals. *J. Phys. Org. Chem.* **2018**, *31*, No. e3836.

(3) Bentley, R.; Chasteen, T. G. Environmental VOSCs−−formation and degradation of dimethyl sulfide, methanethiol and related materials. *Chemosphere* **2004**, *55*, 291−317.

(4) Hu, H.; Mylon, S. E.; Benoit, G. Volatile organic sulfur compounds in a stratified lake. *Chemosphere* **2007**, *67*, 911−919.

(5) Aneja, V. P.; Cooper, W. J. Biogenic Sulfur Emissions: a Review. In *Biogenic Sulfur in the Environment*; Saltzman, E. S.; Cooper, W. J., Eds.; ACS Symposium Series 393; American Chemical Society: Washington, DC, 1989; Chapter 1−13.

(6) Andreae, M. O.; Andreae, T. W. The cycle of biogenic sulfur compounds over the Amazon basin: 1. dry season. *J. Geophys. Res.* **1988**, *93*, 1487−1497.

(7) Delmas, R.; Baudet, J.; Servant, J.; Baziard, Y. Emissions and concentrations of hydrogen sulfide in the air of the tropical forest of the Ivory Coast and of temperate regions in France. *J. Geophys. Res.* **1980**, *85*, 4468−4474.

(8) Lamb, B.; Westberg, H.; Allwine, G.; Bamesberger, L.; Guenther, A. Measurement of biogenic sulfur emissions from soils and vegetation: Application of dynamic enclosure methods with Natusch filter and GC/FPD analysis. *J. Atmos. Chem.* **1987**, *5*, 469−491.

(9) Wilson, L. G.; Bressan, R. A.; Filner, P. Light-dependent emission of hydrogen sulfide from plants. *Plant Physiol.* **1978**, *61*, 184−189.

(10) Puxbaum, H.; König, G. Observation of dipropenyldisulfide and other organic sulfur compounds in the atmosphere of a beech forest with Allium ursinum ground cover. *Atmos. Environ.* **1997**, *31*, 291−294.

(11) Oaks, D. M.; Hartmann, H.; Dimick, K. P. Analysis of sulfur compounds with electron capture/hydrogen flame dual channel gas chromatography. *Anal. Chem.* **1964**, *36*, 1560−1565.

(12) Block, E.; Putman, D.; Zhao, S. H. Allium chemistry: GC-MS analysis of thiosulfinates and related compounds from onion, leek, scallion, shallot, chive, and Chinese chive. *J. Agric. Food Chem.* **1992**, *40*, 2431−2438.

(13) Arathala, P.; Musah, R. A. Theoretical studies of the gas-phase reactions of S-methyl methanesulfinothioate (dimethyl thiosulfinate) with OH and Cl radicals: Reaction mechanisms, energetics, and kinetics. *J. Phys. Chem. A* **2019**, *123*, 8448−8459.

(14) Li, S.; Matthews, J.; Sinha, A. Atmospheric hydroxyl radical production from electronically excited NO_2 and H_2O. *Science* **2008**, *319*, 1657−1660.

(15) Hofzumahaus, A.; Rohrer, F.; Lu, K.; Bohn, B.; Brauers, T.; Chang, C.-C.; Fuchs, H.; Holland, F.; Kita, K.; Kondo, Y.; et al. Amplified trace gas removal in the troposphere. *Science* **2009**, *324*, 1702−1704.
(16) Riedel, K.; Lassey, K. Detergent of the atmosphere. *Water Atmos.* **2008**, *16*, 22−23.
(17) Glowacki, D. R.; Liang, C.-H.; Morley, C.; Pilling, M. J.; Robertson, S. H. MESMER: an open-source master equation solver for multi-energy well reactions. *J. Phys. Chem. A* **2012**, *116*, 9545−9560.
(18) Frisch, M. J.; Trucks, G. W.; Schlegel, H. B.; Scuseria, G. E.; Robb, M. A.; Cheeseman, J. R.; Scalmani, G.; Barone, V.; Petersson, G. A.; Nakatsuji, H.; et al. *Gaussian 16*, Revision B.01; Gaussian, Inc.: Wallingford, CT, 2016.
(19) Peverati, R.; Truhlar, D. G. Quest for a universal density functional: The accuracy of density functionals across a broad spectrum of databases in chemistry and physics. *Philos. Trans. R. Soc., A* **2014**, *372*, 20120476.
(20) Parandaman, A.; Tangtartharakul, C. B.; Kumar, M.; Francisco, J. S.; Sinha, A. A computational study investigating the energetics and kinetics of the HNCO + $(CH_3)_2NH$ reaction catalyzed by a single water molecule. *J. Phys. Chem. A* **2017**, *121*, 8465−8473.
(21) Parandaman, A.; Kumar, M.; Francisco, J. S.; Sinha, A. Organic acid formation from the atmospheric oxidation of gem diols: Reaction mechanism, energetics, and rates. *J. Phys. Chem. A* **2018**, *122*, 6266−6276.
(22) Zhao, Y.; Truhlar, D. G. Density functionals with broad applicability in chemistry. *Acc. Chem. Res.* **2008**, *41*, 157−167.
(23) Fukui, K. The path of chemical reactions - the IRC approach. *Acc. Chem. Res.* **1981**, *14*, 363−368.
(24) Hratchian, H. P.; Schlegel, H. B., Chapter 10 - Finding minima, transition states, and following reaction pathways on ab Initio potential energy surfaces. In *Theory and Applications of Computational Chemistry*; Dykstra, C. E., Frenking, G., Kim, K. S., Scuseria, G. E., Eds.; Elsevier: Amsterdam, 2005; pp 195−249.
(25) Noga, J.; Bartlett, R. J. The full CCSDT model for molecular electronic structure. *J. Chem. Phys.* **1987**, *86*, 7041−7050.
(26) Schlegel, H. B.; Sosa, C. Ab initio molecular orbital calculations on $F+H_2 \rightarrow HF+H$ and $OH+H_2 \rightarrow H_2O+H$ using unrestricted Møller-Plesset perturbation theory with spin projection. *Chem. Phys. Lett.* **1988**, *145*, 329−333.
(27) Ignatyev, I. S.; Xie, Y.; Allen, W. D.; Schaefer, H. F. Mechanism of the $C_2H_5+O_2$ reaction. *J. Chem. Phys.* **1997**, *107*, 141−155.
(28) Arathala, P.; Katz, M.; Musah, R. A. Reaction mechanism, energetics, and kinetics of the water-assisted thioformaldehyde + $\dot{O}H$ reaction and the fate of its product radical under tropospheric conditions. *Phys. Chem. Chem. Phys.* **2020**, *22*, 10027−10042.
(29) Parandaman, A.; Perez, J. E.; Sinha, A. Atmospheric decomposition of trifluoromethanol catalyzed by formic acid. *J. Phys. Chem. A* **2018**, *122*, 9553−9562.
(30) Carr, S. A.; Still, T. J.; Blitz, M. A.; Eskola, A. J.; Pilling, M. J.; Seakins, P. W.; Shannon, R. J.; Wang, B.; Robertson, S. H. Experimental and theoretical study of the kinetics and mechanism of the reaction of OH radicals with dimethyl ether. *J. Phys. Chem. A* **2013**, *117*, 11142−11154.
(31) Zhao, X.; Wang, L. Atmospheric oxidation mechanism of furfural initiated by hydroxyl radicals. *J. Phys. Chem. A* **2017**, *121*, 3247−3253.
(32) Bartis, J. T.; Widom, B. Stochastic models of the interconversion of three or more chemical species. *J. Chem. Phys.* **1974**, *60*, 3474−3482.
(33) Robertson, S. H.; Pilling, M. J.; Jitariu, L. C.; Hillier, I. H. Master equation methods for multiple well systems: Application to the 1-,2-pentyl system. *Phys. Chem. Chem. Phys.* **2007**, *9*, 4085−4097.
(34) Miller, J. A.; Klippenstein, S. J.; Robertson, S. H.; Pilling, M. J.; Green, N. J. B. Detailed balance in multiple-well chemical reactions. *Phys. Chem. Chem. Phys.* **2009**, *11*, 1128−1137.
(35) Klippenstein, S. J.; Miller, J. A. From the time-dependent, multiple-well master equation to phenomenological rate coefficients. *J. Phys. Chem. A* **2002**, *106*, 9267−9277.
(36) Sun, T.; Teja, A. S. An equation of state for real fluids based on the Lennard-Jones potential. *J. Phys. Chem.* **1996**, *100*, 17365−17372.
(37) Nicovich, J. M.; Mazumder, S.; Laine, P. L.; Wine, P. H.; Tang, Y.; Bunkan, A. J. C.; Nielsen, C. J. An experimental and theoretical study of the gas phase kinetics of atomic chlorine reactions with CH_3NH_2, $(CH_3)_2NH$, and $(CH_3)_3N$. *Phys. Chem. Chem. Phys.* **2015**, *17*, 911−917.
(38) Miller, W. H. Tunneling corrections to unimolecular rate constants, with application to formaldehyde. *J. Am. Chem. Soc.* **1979**, *101*, 6810−6814.
(39) Blitz, M. A.; Hughes, K. J.; Pilling, M. J.; Robertson, S. H. Combined experimental and master equation investigation of the multiwell reaction H + SO_2. *J. Phys. Chem. A* **2006**, *110*, 2996−3009.
(40) Atkinson, R. Atmospheric chemistry of VOCs and NOx. *Atmos. Environ.* **2000**, *34*, 2063−2101.
(41) Pinnock, S.; Hurley, M. D.; Shine, K. P.; Wallington, T. J.; Smyth, T. J. Radiative forcing of climate by hydrochlorofluorocarbons and hydrofluorocarbons. *J. Geophys. Res.* **1995**, *100*, 23227−23238.
(42) EPI. *AOPWIN* v.1.92 Atmospheric Oxidation Program for Microsoft Windows; U.S. Environmental Protection Agency, 2000.
(43) Long, B.; Bao, J. L.; Truhlar, D. G. Reaction of SO_2 with OH in the atmosphere. *Phys. Chem. Chem. Phys.* **2017**, *19*, 8091−8100.
(44) Rowland, F. S. Stratospheric ozone depletion. *Philos. Trans. R. Soc., B* **2006**, *361*, 769−790.
(45) Webster, C. R.; May, R. D.; Jaeglé, L.; Hu, H.; Sander, S. P.; Gunson, M. R.; Toon, G. C.; Russell, J. M., III; Stimpfle, R. M.; Koplow, J. P.; et al. Hydrochloric acid and the chlorine budget of the lower stratosphere. *Geophys. Res. Lett.* **1994**, *21*, 2575−2578.
(46) Lee, T. J.; Taylor, P. R. A diagnostic for determining the quality of single-reference electron correlation methods. *Int. J. Quantum Chem., Symp.* **1989**, *36*, 199−207.
(47) Bianchi, F.; Kurtén, T.; Riva, M.; Mohr, C.; Rissanen, M. P.; Roldin, P.; Berndt, T.; Crounse, J. D.; Wennberg, P. O.; Mentel, T. F.; et al. Highly oxygenated organic molecules (HOM) from gas-phase autoxidation involving peroxy radicals: A key contributor to atmospheric aerosol. *Chem. Rev.* **2019**, *119*, 3472−3509.

https://dx.doi.org/10.1021/acs.jpca.0c05200
J. Phys. Chem. A 2020, 124, 8292−8304